ADVANCED OPTICAL MATERIALS
www.advopticalmat.de

Check for updates

Controlling Charge Accumulation Properties of Organic Light-Emitting Diodes using Dipolar Doping of Hole Transport Layers

Yutaka Noguchi, Alexander Hofmann, and Wolfgang Brütting**

It is demonstrated that dipolar doping of hole transport layers (HTLs) controls the density and polarity of the accumulated charge at the critical interface between the HTL and the emission layer (EML) in organic light-emitting diodes (OLEDs). Dipolar doping enables spontaneous orientation polarization (SOP) even in nonpolar HTL, and consequently compensates for the negative interface charge originating from the SOP of the adjacent layer. This concept is applied to a phosphorescent OLED, where bis-4(*N*-carbazolyl) phenylphosphine oxide (BCPO) is employed as a polar dopant for the HTL. The net interface charge is completely compensated at ≈29.5% of doping and further doping even facilitates the positive interface charge. The luminescence loss due to triplet-polaron quenching is observed for both hole and electron accumulations, and it is suppressed by reducing the net interface charge density. On the other hand, the carrier balance factor linearly decreases with increasing doping ratio of BCPO. The results suggest that besides the energy level offset, SOP and permanent dipole moment of the materials should also be taken into account for realizing efficient carrier blocking interfaces. Dipolar doping is a versatile tool to tune charge accumulation, and to study its influence on device performance as well as the role of SOP in OLEDs.

1. Introduction

Controlling charge accumulation at interfaces is an important issue to optimize device performance of organic light-emitting diodes (OLEDs), since it influences key device parameters, such as the external quantum efficiency (EQE), efficiency roll-off, and device degradation.[1–9] Although the charge accumulation properties at organic hetero interfaces have been often discussed in terms of the energy barrier to charge injection, it is known that the interface charge due to spontaneous orientation polarization (SOP) also plays a significant role.[5,9–12] SOP originates from the macroscopic polarization induced by partial alignment of the permanent dipole moments (PDMs) of polar organic semiconducting materials in evaporated films,[9,13,14] and dominates the charge accumulation properties below the turn-on voltage of OLEDs.[5,15,16] SOP has been frequently observed in many common OLED materials, particularly emitters and electron transport materials, though it is very small in most hole transport materials.[5,17–19]

Recently, Bangsund et al. have demonstrated that the excess charge accumulation due to SOP can reduce the EQE of OLEDs via exciton-polaron quenching, and EQE can be enhanced by eliminating SOP in the device.[6] Thus far, substrate heating during deposition and use of materials with negligible SOP have been examined to eliminate the excess charge accumulation.[6,7] However, substrate heating can influence the properties of underlayers in the device stack, since SOP is often formed in an emission layer (EML) and electron transport layer (ETL) that are commonly deposited on a hole transport layer (HTL). On the other hand, employing negligible SOP materials limits the possible choice of materials and would not be the best for the overall performance of OLEDs. For instance, many phosphorescent and thermally activated delayed fluorescence emitters also exhibit SOP, and ETL materials with negligible SOP are limited.[5,17] As an alternative method, Afolayan et al. have reported very recently that SOP is efficiently eliminated in a co-evaporated film of ETL and medium density of polyethylene.[8] They demonstrated a higher EQE and longer lifetime of a blue OLED by eliminating the SOP of the ETL. Meanwhile, the benefits of SOP in OLEDs are still controversial, e.g., SOP can improve charge injection efficiency and also affect charge blocking property.[20–24] Thus, exploring methods to control the charge accumulation property while keeping SOP is an important issue to optimize the device performance as well as to understand the role of SOP. In that sense, it will be intriguing to use a device stack with identical

Y. Noguchi
School of Science & Technology
Meiji University
Kawasaki 214-8571, Japan
E-mail: noguchi@meiji.ac.jp

A. Hofmann, W. Brütting
Institute of Physics
University of Augsburg
86135 Augsburg, Germany
E-mail: bruetting@physik.uni-augsburg.de

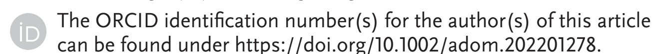
The ORCID identification number(s) for the author(s) of this article can be found under https://doi.org/10.1002/adom.202201278.

© 2022 The Authors. Advanced Optical Materials published by Wiley-VCH GmbH. This is an open access article under the terms of the Creative Commons Attribution-NonCommercial License, which permits use, distribution and reproduction in any medium, provided the original work is properly cited and is not used for commercial purposes.

DOI: 10.1002/adom.202201278

 © 2022 The Authors. Advanced Optical Materials published by Wiley-VCH GmbH

21951071, 2022, 21, Downloaded from https://onlinelibrary.wiley.com/doi/10.1002/adom.202201278 by Universitaetsbibl Augsburg, Wiley Online Library on [06/11/2022]. See the Terms and Conditions (https://onlinelibrary.wiley.com/terms-and-conditions) on Wiley Online Library for rules of use; OA articles are governed by the applicable Creative Commons License

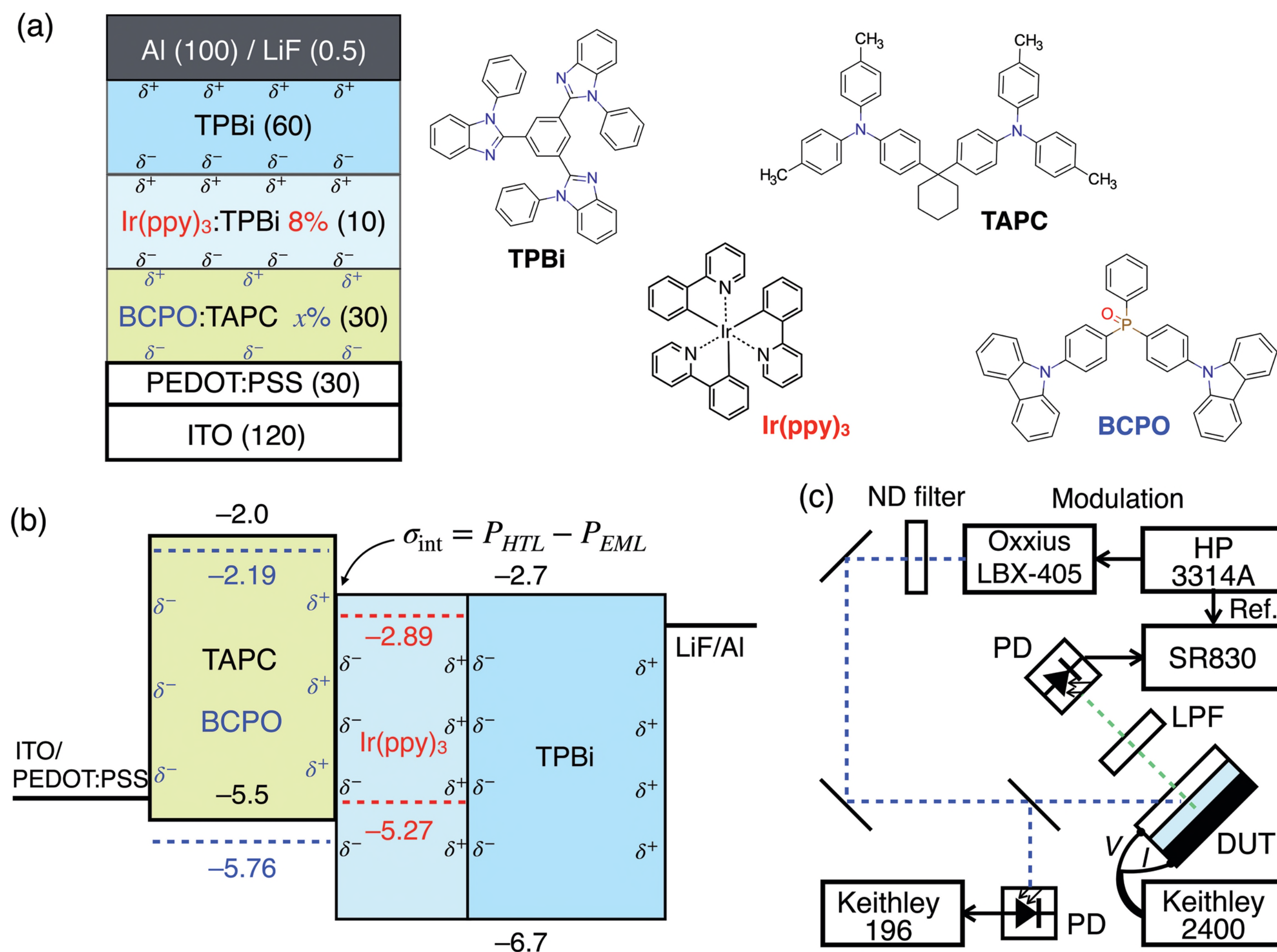

Figure 1. a) Schematic illustration of the device structure under study. The number in parentheses indicates the film thickness in nm. $\delta^{+/-}$ indicates positive/negative polarization charge due to SOP. The chemical structure of the molecules is also shown. b) Schematic energy diagram of the device. The highest occupied molecular orbital (HOMO) and lowest unoccupied molecular orbital (LUMO) levels of each material are indicated in eV (relative to the vacuum level). The net interface charge density (σ_{int}) at the HTL/EML interface is given by the difference of SOPs of HTL (P_{HTL}) and EML (P_{EML}). c) The experimental setup for the PL intensity measurement under applied electric bias. A laser diode module (Oxxius, LBX-405) at a wavelength of 405 nm is used as an excitation light source, where the intensity is modulated by a function generator (HP 3314A) at a frequency of 719 Hz. The actual laser intensity is monitored by a digital multimeter (Keithley 196), and the PL intensity from the device is detected by a lock-in amplifier (SR830). A biasing voltage is applied to the device and current is measured by a source measure unit (Keithley 2400).

(non-vanishing) SOP in all layers. However, this requires the use of HTLs exhibiting SOP.

In this study, we propose a method to control charge accumulation using dipolar doping of HTLs. Dipolar doping has been proposed by Jäger et al. to control SOP of mixed films of tris-(8-hydroxyquinolate) aluminum (Alq_3) and *N*,*N*″-bis(1-naphthyl)-*N*,*N*″-diphenyl-1,1″-biphenyl-4,4″-diamine (NPB),[25] where Alq_3 is a typical polar material exhibiting SOP,[26] while NPB is almost nonpolar.[16] They demonstrated that the SOP of the mixed film depends on the concentration of Alq_3. Remarkably, the largest SOP was observed at a mixing ratio of ≈50%, because of the enhancement of the orientation degree of the PDM of Alq_3 by reducing their mutual dipole-dipole interaction. Hofmann et al. applied mixed films of Alq_3 and NPB as an HTL that possesses SOP, and demonstrated that the dipolar doped HTL enhances hole injection efficiency.[22] Although intrinsic HTLs typically exhibit only small SOP, dipolar doping can facilitate SOP in HTLs. The polarization charge of a dipolar doped HTL compensates for the interface charge originating from the SOP of the adjacent layer, e.g., emission layer (EML).[5,16,19] Consequently, the dipolar doped HTL enables us to control the density and even polarity of the accumulated charge without changing the properties of other layers in the device stack.

We examined this concept of using dipolar doped HTLs in a tris(2-phenylpyridine) iridium(III) ($Ir(ppy)_3$)-based OLED, where 1,3,5-tris(1-phenyl-1H-benzimidazol-2-yl)benzene (TPBi), a typical SOP material, is used as ETL and the host of the EML (**Figure 1**a,b). Here, bis-4-(*N*-carbazolyl)phenylphosphine oxide (BCPO) was employed as a dopant to facilitate SOP in an HTL consisting of 4,4′-cyclohexylidenebis[*N*,*N*- bis(4-methylphenyl)benzenamine] (TAPC) as the host. Note that BCPO was chosen as a dipolar dopant because neat films of this material were found to exhibit record-high SOP in previous studies.[18] The capacitance-voltage (*C*–*V*) curves of these devices clearly

© 2022 The Authors. Advanced Optical Materials published by Wiley-VCH GmbH

21951071, 2022, 21, Downloaded from https://onlinelibrary.wiley.com/doi/10.1002/adom.202201278 by Universitaetsbibl Augsburg, Wiley Online Library on [06/11/2022]. See the Terms and Conditions (https://onlinelibrary.wiley.com/terms-and-conditions) on Wiley Online Library for rules of use; OA articles are governed by the applicable Creative Commons License

21951071, 2022, 21, Downloaded from https://onlinelibrary.wiley.com/doi/10.1002/adom.202201278 by Universitaetsbibl Augsburg, Wiley Online Library on [06/11/2022]. See the Terms and Conditions (https://onlinelibrary.wiley.com/terms-and-conditions) on Wiley Online Library for rules of use; OA articles are governed by the applicable Creative Commons License

indicate that the accumulated hole density decreases with increasing doping ratio of BCPO, and at 29.5%, the net interface charge at the HTL/EML interface was almost completely compensated. Further doping flipped the polarity of the interface charge toward positive, thus inducing electron accumulation at the HTL/EML interface. Photoluminescence (PL) measurements[6,27] (Figure 1c) reveal that both holes and electrons accumulated at the HTL/EML interface contribute to triplet-polaron quenching (TPQ), though the rate constant of TPQ for electrons is ≈1/3 of that for holes. Importantly, a significant PL quenching occurred below the turn-on voltage of the OLED, and the total accumulated charge, rather than the actual device current, is considered as a main quencher in these devices also above turn-on. On the other hand, the EQE did not simply increase with reducing the accumulated charge density. We found that the carrier balance factor linearly declined with the enhancing SOP of the HTL, and it can be attributed to a deterioration of the electron blocking ability at the HTL/EML interface. Despite the drawback of electron leakage, the EQE of the doped devices can be higher than that of the un-doped device, particularly at high current densities. Moreover, the results suggest that besides the energy level offset, SOP and PDM of the materials should be taken into account for realizing efficient carrier blocking interfaces. Dipolar doping can therefore be widely applied to modify the charge accumulation properties of OLEDs, and is useful to investigate the influence of charge accumulation on the device performance as well as the role of SOP in OLEDs.

2. Results

2.1. Charge Accumulation Properties

Figure 2a shows the *C–V* curves at a frequency of 10 Hz. A transition from depletion to accumulation appears at a distinct voltage, namely the injection voltage (V_{inj}, marked by a triangle in Figure 2a), which is clearly below the turn-on voltage of the device (V_{th}≈2.4 V for all devices), because of the presence of an interface charge.[5,10–12] Upon BCPO doping of the TAPC HTL, we observe a shift of V_{inj} to the positive side up to a doping ratio of 29.5%; but further increase of the doping concentration leads to a negative shift. At the same time, the capacitance of the accumulation state also changes to higher values after flipping the direction of the V_{inj} shift. These results clearly demonstrate that dipolar doping controls the charge accumulation properties of the device.

The geometrical capacitance of the whole device is estimated to be 1.06 nF, corresponding to the capacitance of the depletion state (before charge injection). Meanwhile, assuming that the HTL/EML interface is responsible for the charge accumulation, the capacitance of the hole and electron accumulation states is estimated to be 1.52 and 3.54 nF, respectively. These capacitances are calculated from the film thicknesses (Figure 1a), the active device area (0.04 cm^2), and the dielectric constant. Here, the relative dielectric constant of all organic semiconducting layers is assumed to be 3, and the contribution of the poly(3,4-ethylenedioxythiophene) polystyrene sulfonate (PEDOT:PSS) layer to the capacitance is omitted. Although there are quantitative discrepancies between estimated and measured capacitances, it is reasonable to conclude that the accumulated charges change from holes to electrons at doping ratios higher than 29.5%.

Figure 2b shows the capacitance-frequency (*C–f*) curves of the devices at a dc offset voltage of 2.5 V, i.e., only slightly above the device turn-on voltage. The relaxation frequency (f_r), which corresponds to the inverse of the RC time constant of the conductive layer (see Supporting Information),[28] is marked by a triangle in Figure 2b. Since the capacitance is considered to be constant, f_r is proportional to the conductance. In Figure 2b, f_r shifts to the lower side as the doping ratio is increased, and the lowest value (7.1 Hz) is observed at the critical value of 29.5% doping. Then, the relaxation frequency shifts again to a higher value (165.8 Hz) at a 40.4% doping, but only slightly increases for further doping (245.6 Hz at 52.8%). These results indicate that the resistance of the responsible layer for the charge transport significantly depends on the doping ratio in case it is lower than 29.5%. It is again reasonable because the responsible layer changes from the HTL to the ETL after flipping the polarity of the majority carrier, and the dipolar doping only affects the conductance of the HTL.

The interface charge density was evaluated by integrating *C–V* curves from V_{inj} to V_{th} (Figure 2c).[5,6,15,16] The broken line indicates the calculated interface charge density from the giant surface potential (GSP) slopes reported previously for each material (see Experimental section). Here, we assumed

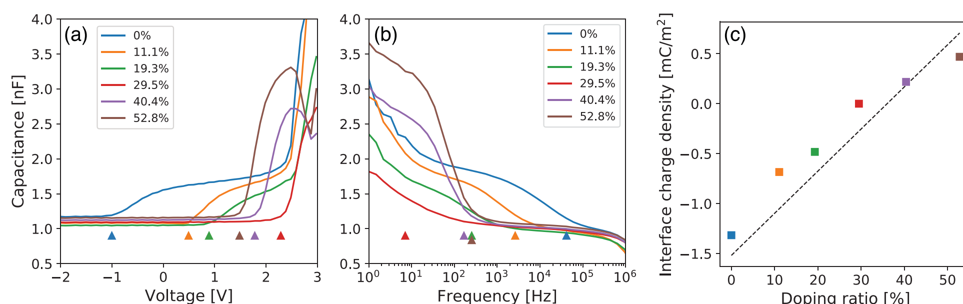

Figure 2. a) Capacitance-voltage (*C–V*) curves of the device with different BCPO doping ratios at a frequency of 10 Hz. The injection voltage (V_{inj}) of each curve is marked by a triangle, where the color corresponds to the doping ratio. b) Capacitance-frequency curves at a dc offset voltage of 2.5 V. The relaxation frequency of each curve is marked by a triangle. c) Interface charge density evaluated by integrating the *C–V* curve of each device. The color indicates the doping ratio of BCPO. The broken line indicates the interface charge density calculated from the GSP slopes reported previously (see Supporting Information).

© 2022 The Authors. Advanced Optical Materials published by Wiley-VCH GmbH

that the orientation degree of PDMs is constant regardless of the doping ratio of BCPO. Although the enhancement of the degree of orientation has been often observed in mixed films,[25,29,30] such effect seems to be small for the BCPO:TAPC films because the experimentally obtained values are close to the calculated ones.

The enhancement of the orientation degree in mixed films usually originates from the reduction of their mutual dipole-dipole interaction by diluting the PDM density.[25,30] However, BCPO has a very large orientation degree (0.33) compared to other SOP materials ever reported (typically < 0.1) even in the neat film.[18] The driving force of the anisotropic molecular orientation of BCPO, that is mainly the van der Waals interaction on the film surface,[31] is expected to be much stronger than the PDM interaction. Accordingly, the orientation degree of BCPO was not enhanced in the BCPO:TAPC film even though the PDM interaction was further weakened by dilution.

2.2. Triplet-Polaron Quenching

Figure 3a shows the normalized PL intensity as a function of applied voltage. The experimental setup is shown in Figure 1c. The PL intensity decays at voltages already below V_{th}, and its onset voltage changes similar to V_{inj} in the C–V curve, indicating that the accumulated charge is responsible for the PL quenching. About 20% of PL efficiency is lost below V_{th} in the un-doped device, and this behavior agrees well with previously reported observations.[6,8] Remarkably, dipolar doping reduces the PL efficiency loss by eliminating the accumulated hole density, and the least PL efficiency loss at V_{th} is observed for the 40.4%-doped device, though it is almost the same for the 29.5%-doped device. Further dipolar doping (52.8%) leads to an even steeper PL efficiency loss, but now due to the electron accumulation. We note here that the discrepancies between the C–V characteristics (Figure 2a) and normalized PL intensity curves (Figure 3a), such as the onset voltage of the PL decay and V_{inj} and almost the same PL losses in some devices (11.1% and 19.3%, 29.5% and 40.4%) may originate from the details of the accumulated charge distribution in the device. TPQ depends strongly on the spatial charge distribution in the EML and around the HTL/EML interface region defined by the Förster radius, though the capacitance is influenced by the charge distribution throughout the device. Accordingly, the PL intensity curve of some devices does not exactly follow the results of the C–V curve.

It is also visible that in all devices (except the 29.5% and 40.4%-doped ones), the slope of the normalized PL intensity changes above V_{th}, indicating that bipolar charge injection changes the charge distribution in the devices. The normalized PL intensities are also plotted as a function of current density in Figures 3b,c. The rapid PL loss occurs at the zero current region (< 10^{-4} mA cm^{-2}, Figure 3c), corresponding to the applied voltages below V_{th}. In this range, the detected current is just a parasitic leakage current, because the actual device current drops exponentially below V_{th} (see **Figure 4**a), whereas the PL loss above V_{th} depends only weakly on the current density (Figure 3b). Overall PL decay curves linearly depend on the applied voltage (Figure 3a), suggesting that the total accumulated charge rather than the actual device current dominates the PL quenching process (see Discussion).

2.3. Current Density–Voltage and Luminance–Voltage Curves

All the doped devices show lower current densities and luminance compared with the un-doped device (Figures 4a,b). The overall shape of the J–V curves changes at a doping ratio between 19.3–29.5%. Around 19.3% BCPO doping, the resistance of the HTL becomes comparable to that of the ETL according to the C–f curves (Figure 2b), and the majority carrier type in the device switches from holes to electrons at the 29.5%-doped device. Accordingly, it is reasonable that the dominant layer of the device resistance changes from the ETL to the HTL at a doping ratio between 19.3–29.5%. We should also mention that the highly doped devices achieve higher current above ≈4 V, which might indicate leakage of electrons into the HTL (see Discussion). Meanwhile, the L–V curves more or less follow the current-voltage characteristics (Figure 4b) at least on this scale.

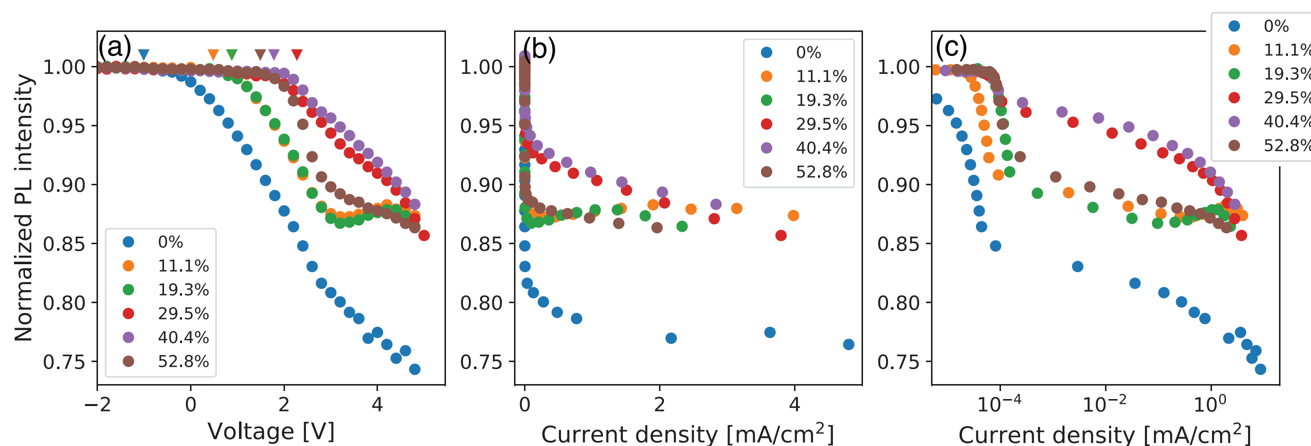

Figure 3. Normalized PL intensity as a function of a) applied voltage, b) current density (linear scale), and c) current density (log-scale). The injection voltage estimated from the C–V curves is marked by an inverted triangle, where the color corresponds to the doping ratio.

 © 2022 The Authors. Advanced Optical Materials published by Wiley-VCH GmbH

21951071, 2022, 21, Downloaded from https://onlinelibrary.wiley.com/doi/10.1002/adom.202201278 by Universitaetsbibl Augsburg, Wiley Online Library on [06/11/2022]. See the Terms and Conditions (https://onlinelibrary.wiley.com/terms-and-conditions) on Wiley Online Library for rules of use; OA articles are governed by the applicable Creative Commons License

21951071, 2022, 21, Downloaded from https://onlinelibrary.wiley.com/doi/10.1002/adom.202201278 by Universitaetsbibl Augsburg, Wiley Online Library on [06/11/2022]. See the Terms and Conditions (https://onlinelibrary.wiley.com/terms-and-conditions) on Wiley Online Library for rules of use; OA articles are governed by the applicable Creative Commons License

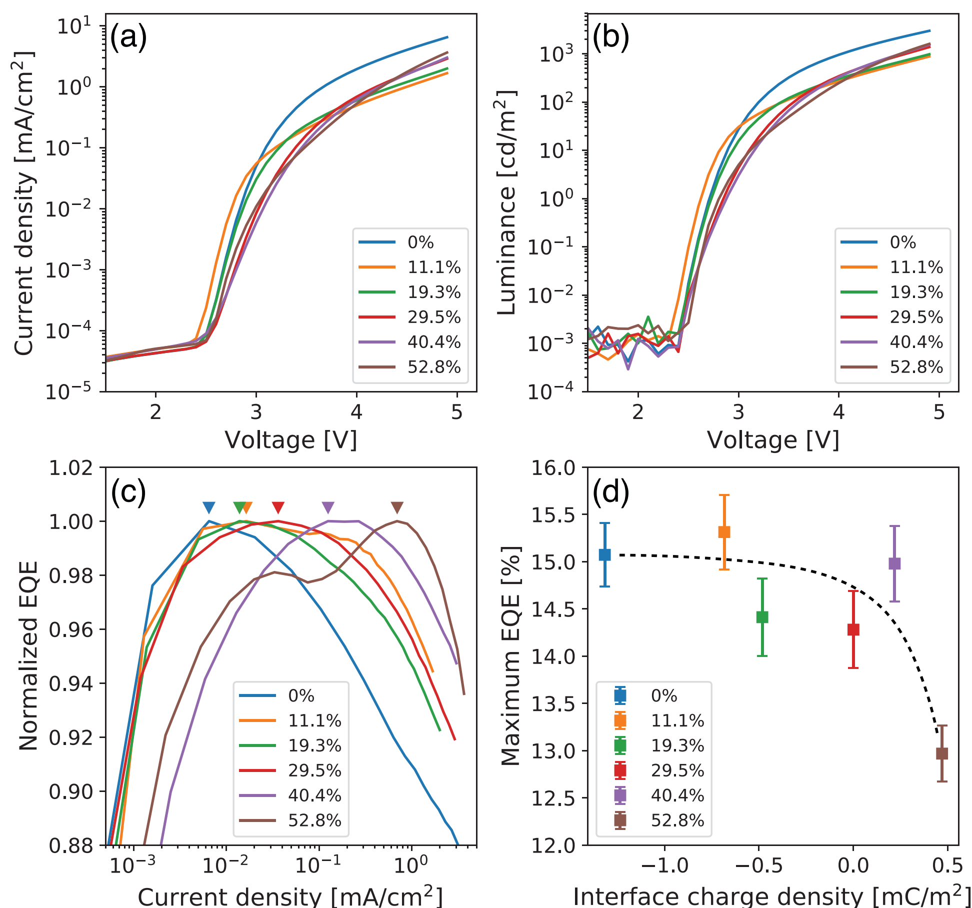

Figure 4. a) Current density-voltage (*J*–*V*) and b) luminance-voltage (*L*–*V*) curves. c) Normalized external quantum efficiency (EQE) as a function of the current density. The current density for the maximum EQE is marked by a triangle, where the color corresponds to the doping ratio. d) Maximum EQE of each device in relation to the interface charge density. The broken line is a guide to the eye.

2.4. External Quantum Efficiency (EQE)

EQE as a function of the current density is shown in Figure 4c, where EQEs are normalized by the maximum value of each device. The current density for the maximum EQE appears at ≈6.5×10^{-3} mA cm^{-2} for the un-doped device, and it shifts to the higher side with increasing doping ratio (Figure 4c, marked by a triangle). Interestingly, there are two maxima of EQE at different current densities in the 52.8%-doped device. These characteristics may result from a combination of the charge accumulation and the electron leakage properties at the HTL/EML interface, where they deteriorate the radiative quantum efficiency and carrier balance factor, respectively (see Discussion). Meanwhile, the maximum EQE of each device is plotted in relation to the interface charge density (Figure 4d). Although the plots are scattered, possibly due to the details of the device fabrication conditions in different batches, the overall trend suggests a lower maximum EQE at a higher doping ratio. However, the highest EQE (15.3%) is observed for the 11.1%-doped device, and the EQE of the doped devices can be higher than that of the un-doped device in some regions of the *J*–*V* characteristics, particularly at high current densities.

3. Discussion

3.1. Charge Accumulation Properties Above the Turn-On Voltage

In terms of the energy diagram and location of the interface charge, it is plausible that the electrons and holes are mainly accumulated at the HTL/EML interface (Figure 1b). The *C*–*V* and *C*–*f* curves reveal that dipolar doping controls the accumulated charge density and its polarity below the turn-on voltage (< ≈2.4 V). On the other hand, the charge accumulation properties above the turn-on voltage can be deduced from the normalized PL intensity (Figure 3), since it can be attributed to TPQ due to the accumulated charge in the EML region. For the 11.1% and 19.3%-doped devices, the normalized PL intensity slightly increases at applied voltages above ≈3 V, indicating that the accumulated hole density decreases. On the other hand, the normalized PL intensities continuously decrease in the other devices, indicating that the hole accumulation is facilitated for the un-doped device, while there is electron accumulation for the 29.8% to 52.8%-doped devices.

Considering a simple equivalent circuit (**Figure 5**a), the accumulated charge density (σ_{acc}) at the HTL/EML interface above the turn-on voltage is determined by the interface

© 2022 The Authors. Advanced Optical Materials published by Wiley-VCH GmbH

21951071, 2022, 21, Downloaded from https://onlinelibrary.wiley.com/doi/10.1002/adom.202201278 by Universitaetsbibl Augsburg, Wiley Online Library on [06/11/2022]. See the Terms and Conditions (https://onlinelibrary.wiley.com/terms-and-conditions) on Wiley Online Library for rules of use; OA articles are governed by the applicable Creative Commons License

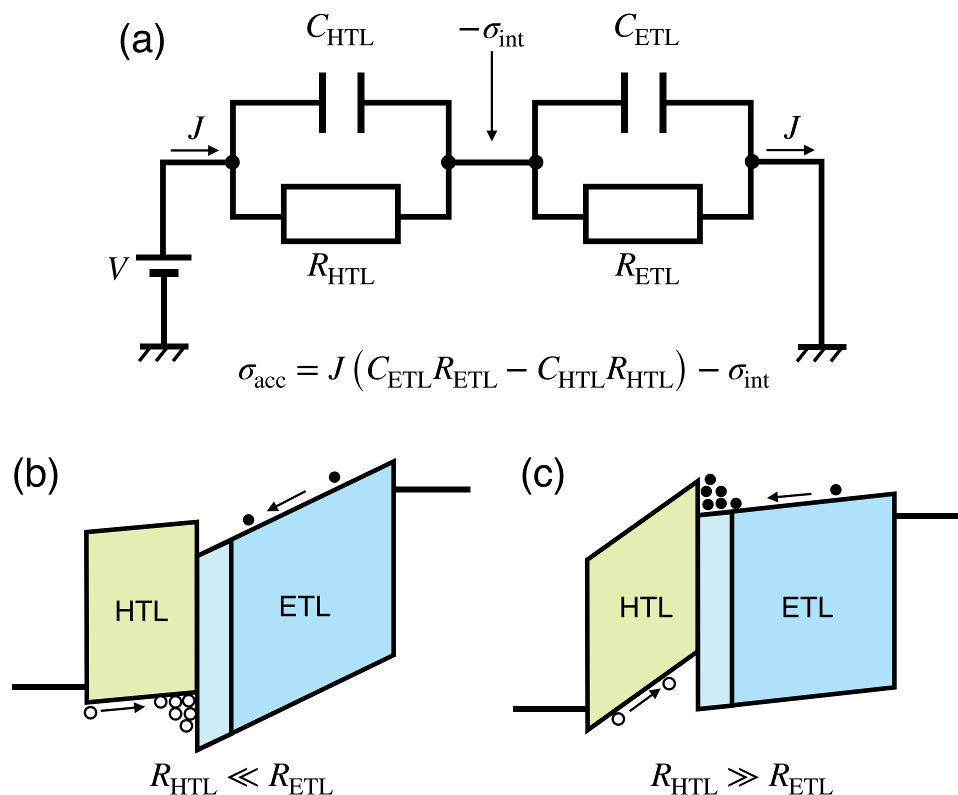

Figure 5. a) A simplified equivalent circuit of the device. The total accumulated charge density at the interface is determined by the difference between the RC time constants of each layer and the interface charge density. b,c) Schematic energy diagram under a bias application (>V_{th}): b) hole and c) electron accumulation is facilitated in case $R_{HTL} \ll R_{ETL}$ and $R_{HTL} \gg R_{ETL}$, respectively.

charge density (σ_{int}) and the difference between the products of the capacitance and the potential drop in each layer, namely $\sigma_{acc}S = C_{ETL}\ V_{ETL} - C_{HTL}V_{HTL} - \sigma_{int}S$, where $C_{ETL(HTL)}$ is the capacitance of the ETL (HTL), and $V_{ETL(HTL)}$ is the potential drop in the ETL (HTL), respectively, and S is the active device area. Here, the EML is incorporated into the ETL for simplicity as both layers mainly consist of TPBi. The equation can be rewritten by using the current density (J) and the resistances ($R_{ETL(HTL)}$) as $\sigma_{acc} = J(C_{ETL}R_{ETL} - C_{HTL}R_{HTL}) - \sigma_{int}$. Accordingly, the difference between the RC time constants of each layer determines how the accumulated charge density develops,[32] e.g., in case R_{HTL} is significantly lower than R_{ETL}, hole accumulation is facilitated (Figure 5b). We note here that $R_{ETL(HTL)}$ includes the resistance for the leakage current, that is the electron (hole) current in the HTL (ETL). As revealed in the C–f curves (Figure 2b), R_{HTL} of the un-doped HTL (neat TAPC layer) is much lower than R_{ETL}, but it is enhanced by the BCPO doping. The 19.3%-doping results in R_{HTL} comparable to R_{ETL}, and for further doping (29.8% and higher), R_{HTL} becomes higher than R_{ETL}, and electron accumulation is facilitated (Figure 5c). These results are qualitatively consistent with those deduced from the normalized PL intensity measurement (Figure 3a). The dipolar doping modifies the charge accumulation characteristics not only below turn-on but also above the turn-on voltage, and such modification would be responsible for the shift of the current density for the maximum EQE (Figure 4c).

3.2. Triplet-Polaron Quenching due to Accumulated Charge

The negative interface charge at the HTL/EML interface forms an electric field that prevents hole injection into the EML at applied voltages between V_{inj} and V_{th}. Accordingly, it is reasonable to assume that holes are mainly located in the HTL. However, some holes may also exist in the EML, although their amount is limited to the interface region because of charge diffusion, thermal, energetical, and structural fluctuations at a practical interface. Comparing the HOMO levels, TAPC and $Ir(ppy)_3$ are likely to capture the holes at the HTL/EML interface, so that TAPC and $Ir(ppy)_3$ cations are possible quenchers in the hole accumulation state. Actually, the absorption band of TAPC and $Ir(ppy)_3$ cations overlaps with the emission band of $Ir(ppy)_3$.[33–35] Note that only TAPC cations that are located roughly within the Förster radius (typically a few nanometers[24]) from the HTL/EML interface can be exciton quenchers.

The TPQ rate constant of $Ir(ppy)_3$ for holes ($k_{TP,h}$) has been reported for different host materials by several groups, and the reported values are widely distributed in the range of 10^{-13} to 10^{-12} cm^3 s^{-1}.[6,36–39] The quantitative difference may be attributed to the different experimental approaches and modeling. Bangsund et al., however, have reported that $k_{TP,h}$ in a TPBi host (3×10^{-13} cm^3 s^{-1}) is ≈40% lower than that in a CBP host (5×10^{-13} cm^3 s^{-1}), where TPBi and 4,4′,4″-tris(N-carbazolyl) triphenylamine (TCTA) was employed as an ETL and HTL, respectively.[6] They pointed out that the lower $k_{TP,h}$ would be

© 2022 The Authors. Advanced Optical Materials published by Wiley-VCH GmbH

attributed to SOP of the EML because it shifts the hole accumulation site from the EML/ETL to the HTL/EML interface, and a portion of the accumulated holes distributes in the TCTA HTL which contributes to less quenching. The normalized PL drop observed in our study quantitatively agrees well with their results,[6] and $k_{TP,h} \approx 3 \times 10^{-13}$ cm^3 s^{-1} is also consistent with our results (see Figure S1, Supporting Information), though the HTL materials are different. Accordingly, the Ir(ppy)$_3$ cation, rather than the TAPC cation, is likely the main quencher in the devices under study.

In the electron accumulation state, the charges may reside in TPBi or Ir(ppy)$_3$ at the HTL/EML interface. Reineke et al. reported that the TPQ rate constant of Ir(ppy)$_3$ for electrons ($k_{TP,e} \approx 2 \times 10^{-13}$ cm^3 s^{-1}) is slightly lower than that for holes ($k_{TP,h} \approx 3 \times 10^{-13}$ cm^3 s^{-1}) in a TCTA host,[36] which is similar to the results obtained in our study ($k_{TP,e} \approx 1 \times 10^{-13}$ cm^3 s^{-1}, and $k_{TP,h} \approx 3 \times 10^{-13}$ cm^3 s^{-1}, see Figure S1, Supporting Information). On the other hand, Oyama et al. reported that Ir(ppy)$_3$ anions have no pronounced absorption within the emission band of Ir(ppy)$_3$, and $k_{TP,e}$ is very small in a CBP host.[38] Thus, a possible quencher in the electron accumulation state would be anions of the host materials rather than Ir(ppy)$_3$. However, comparing the lowest unoccupied molecular orbital (LUMO) levels of these materials, Ir(ppy)$_3$ is most likely to capture electrons, while the host materials are rather unlikely.[40,41] Therefore, further studies are required to identify the quencher in the electron accumulation state.

3.3. EQE and Charge Blocking Properties at the Hole Transport Layer/Emission Layer Interface

Since the PL efficiency loss can be suppressed by eliminating interface charge, the highest EQE is expected for the 29.5%-doped device because of the almost vanishing interface charge density. However, the measured EQEs do not seem to correlate well with the interface charge density (Figure 4d). Since the light-outcoupling efficiency is almost identical for all devices (see Figure S2, Supporting Information), another possible factor to impact on the EQE is the carrier balance.[42] Although the carrier balance factor (γ) cannot be measured directly, it can be derived by dividing the measured EQE by the outcoupling efficiency and the normalized PL intensity at a given current density (**Figure 6**), where the intrinsic radiative quantum efficiency and triplet formation ratio of Ir(ppy)$_3$ were assumed to be unity. Note that γ is normalized by the maximum value for the un-doped device to eliminate quantitative discrepancy between the normalized PL intensity and radiative quantum efficiency that originates from the differences of the exciton distribution in the PL and EL measurements. As shown in Figure 6, the normalized carrier balance factor correlates well with the interface charge density; it decreases approximately linearly with increasing interface charge density.

The deterioration of the carrier balance factor can be attributed to the electron leakage across the HTL/EML interface. To confirm this hypothesis, the current-voltage characteristics of electron only devices (EODs) were examined (**Figure 7**). The device structure of the EODs is the same as for the OLEDs under study (Figure 1a) except for another TPBi layer inserted

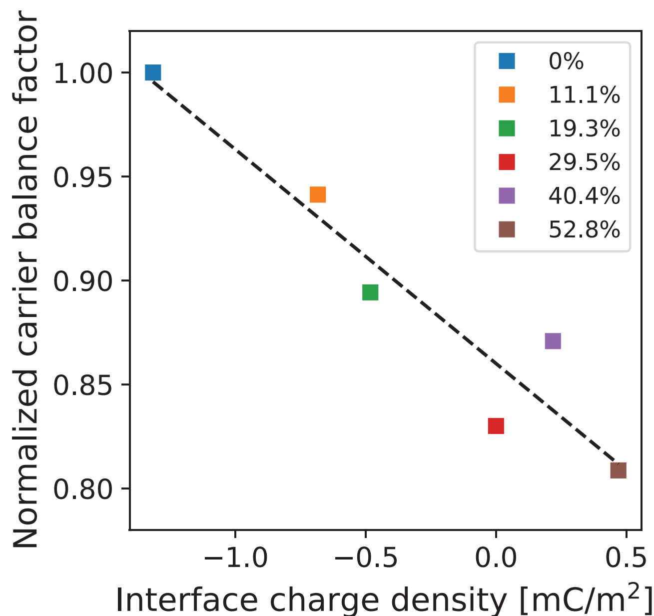

Figure 6. Normalized carrier balance factor at the maximum EQE in relation to the interface charge density. The broken line is a guide to the eye.

between the HTL and the PEDOT:PSS layer as a hole blocking layer (Figure 7a). An electron leakage current was observed for the devices including the doped HTL, whereas this does not happen for the un-doped one (Figure 7b). The shift of the current onset voltage (marked with triangles) is attributed to the elimination of the negative interface charge at the HTL/EML interface. In Figure 7c, the *J*–*V* curves with reference to the onset voltage are shown on a linear scale. The results clearly indicate that the dipolar doping of BCPO induces the electron leakage, and it causes the deterioration of the carrier balance factor in the doped devices.

In addition to the bipolar charge transport nature of BCPO,[43] the electron injection efficiency at the HTL/EML interface should be considered. If we simply consider the LUMO level offset at the HTL/EML interface, the energy barrier of BCPO is lower by ≈0.19 eV than that of TAPC.[44] Although the accurate estimation of the barrier height at actual organic hetero interfaces has been controversial,[45,46] particularly for electrons,[40] there would be an energy offset of ≈0.51 eV between the LUMO levels of BCPO and TPBi according to the typically reported values.[41,47] The electron leakage current across such an interface, as estimated by a device simulation software (Setfos 5.2, FLUXIM AG), is much smaller than the measured current density in the EODs (Figure S3, Supporting Information). However, there would be additional factors to facilitate electron injection at the HTL/EML interface. For instance, the PDM of BCPO (≈3.5 D) induces the density of states (DOS) broadening of HTL, due to the dipolar disorder effect.[24,48,49] The tail states of the broad DOS reduce the effective barrier height at the interface.[49,50] In addition, the presence of a positive polarization charge originating from the SOP of the doped HTL would also enhance the electron injection efficiency. Such an effect has been reported for charge injection at electrode/organic and organic/organic interfaces.[20–24] Thus, the electron leakage

© 2022 The Authors. Advanced Optical Materials published by Wiley-VCH GmbH

21951071, 2022, 21, Downloaded from https://onlinelibrary.wiley.com/doi/10.1002/adom.202201278 by Universitaetsbibl Augsburg, Wiley Online Library on [06/11/2022]. See the Terms and Conditions (https://onlinelibrary.wiley.com/terms-and-conditions) on Wiley Online Library for rules of use; OA articles are governed by the applicable Creative Commons License

21951071, 2022, 21, Downloaded from https://onlinelibrary.wiley.com/doi/10.1002/adom.202201278 by Universitaetsbibl Augsburg, Wiley Online Library on [06/11/2022]. See the Terms and Conditions (https://onlinelibrary.wiley.com/terms-and-conditions) on Wiley Online Library for rules of use; OA articles are governed by the applicable Creative Commons License

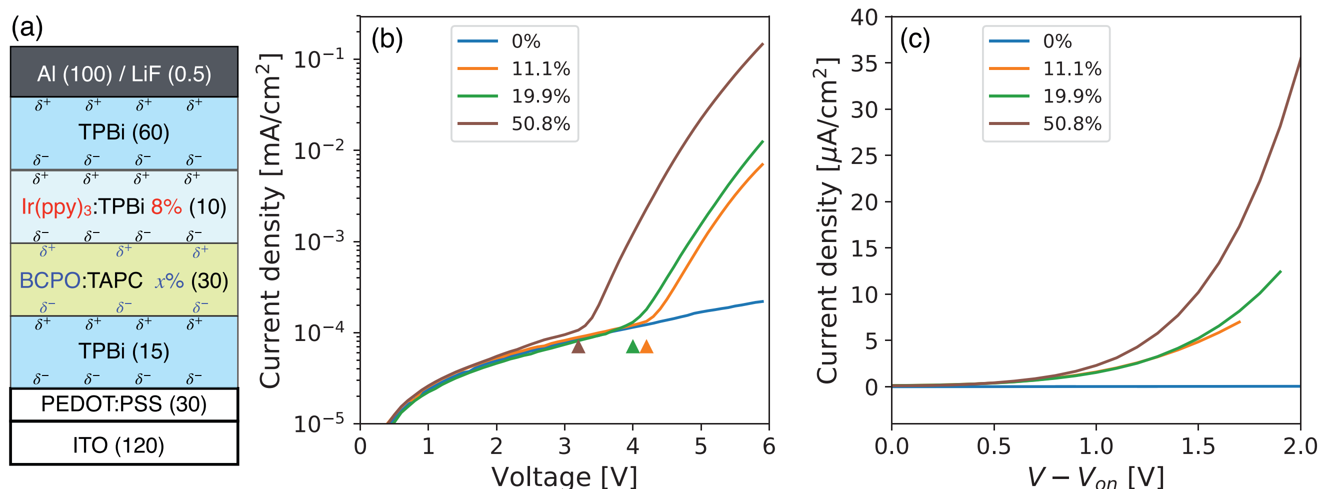

Figure 7. a) Schematic illustration of the structure of the electron only device (EOD). A TPBi layer on the anode side is inserted as a hole blocking layer. The number in parentheses indicates the film thickness in nm. b) Current density-voltage curves of the EODs. The current onset voltage (V_{on}, marked by a triangle) shifts to the negative side because the doped HTL eliminates the negative interface charge at the HTL/EML interface. c) Current density-voltage curves with reference to V_{on}.

current was also simulated using a simplified model[21] as a function of the interface charge density of the HTL (Figure S3, Supporting Information). The simulation result indicates that the interface charge enhances the leakage current on a linear scale, and it is qualitatively consistent with the linear dependence of the carrier balance factor on the interface charge density (Figure 6).

4. Conclusion

We proposed the use of dipolar doping to modify the accumulated charge density and polarity at the interfaces of OLEDs. In this study, the charge accumulation properties of an $Ir(ppy)_3$-based OLED were modified by using dipolar doping of the HTL, namely TAPC doped with BCPO, and the influence on the device properties were investigated. The negative interface charge in the un-doped device, which results in hole accumulation at the HTL/EML interface, was almost completely compensated by the 29.5%-doped HTL and further doping facilitated the formation of a positive interface charge, yielding electron accumulation at the interface. The luminescence loss due to exciton-polaron quenching was suppressed by reducing the net interface charge density at the HTL/EML interface. Meanwhile, the carrier balance factor decreases linearly with increasing SOP of the HTL due to less electron blocking ability at that interface. Although the dipolar doping deteriorates the carrier balance factor, it can shift the current density for the maximum EQE to the higher side, and the EQE can be higher than that of the un-doped device at high current densities. Such optimization of the device operation would be an advantage of using dipolar doped HTLs. Moreover, our results suggest that besides the energy level offset, the dipolar disorder effect and SOP should be considered to realize efficient carrier blocking interfaces. We anticipate that dipolar doping can be applied to any other layer to tune charge accumulation at interfaces, and it is therefore very useful to investigate the influences of charge accumulation on the device performance as well as the role of SOP in OLEDs.

5. Experimental Section

Materials: BCPO was employed as a dopant to facilitate SOP in a TAPC HTL. BCPO is a polar material with a high triplet energy of 3.01 eV,[43] and is known as a material exhibiting very large SOP.[18] Moreover, it was unlikely to act as a hole trap in TAPC, since its HOMO level was deeper than that of TAPC (Figure 1b).[44] TPBi was used as an ETL and a host material of the EML, and $Ir(ppy)_3$ as an emitter. All these materials are polar and exhibit more or less SOP.[5,17–19,30,33] The GSP slopes of neat films of these materials have been reported as 4.3 mV nm^{-1} (TAPC),[33] 163 mV nm^{-1} (BCPO),[18] −3.6 mV nm^{-1} ($Ir(ppy)_3$),[5] and 63 mV nm^{-1} (TPBi).[30] Here, SOP corresponds to the product of the GSP slope and the dielectric constant,[5] which is similar (relative dielectric constant ≈3) in all these materials.

Device Fabrication: The PEDOT:PSS (CLEVIOS P VP CH 8000, Heraeus Deutschland GmbH & Co. KG) film was spin-coated onto a precleaned indium tin oxide (ITO)-coated glass substrate at 5000 rpm for 30 s. After spin-coating, the film was annealed at 125 °C for 40 min. All other organic films were successively deposited using a conventional thermal evaporation technique without controlling substrate temperature at a deposition rate of 1–1.5 Å s^{-1} followed by LiF and Al deposition. The thicknesses of each layer are shown in Figure 1a. The dimensions of the device active area are 0.2×0.2 cm^2.

Device Characterization: The *C*–*V* and *C*–*f* curves were measured by an electrical and optical characterization platform (Paios, FLUXIM AG). The *J*–*V* and *L*–*V* curves were measured by a 2-channel source-measure unit (Keithley 2602B, Keithley Instruments, Inc.) with a calibrated modular light detector (PD-9302-VL, Gigahertz-Optik, GmbH.). All above measurements were performed in a N_2-filled glove box at room temperature. The PL measurement was performed in air after encapsulation of the devices. The experimental setup is illustrated in Figure 1c. The PL intensity was measured by a photodiode (SM1PD1B, Thorlabs, Inc.) through a long pass filter (LPF) with a cut-in wavelength of 450 nm using a lock-in detection technique as a function of applied voltage (SR830, Stanford Research Systems, Inc., and Keithley 2400, Keithley Instruments, Inc.). A laser diode module with a wavelength of 405 nm (LBX-405, Oxxius) was used to excite only $Ir(ppy)_3$ in the devices, where the averaged power density and modulation frequency was

© 2022 The Authors. Advanced Optical Materials published by Wiley-VCH GmbH

≈1 mW cm^{-2} and 719 Hz, respectively. The laser intensity was monitored by a digital multimeter (Keithley 196, Keithley Instruments, Inc), and the modulation was given by a function generator (3314A, Hewlett Packard, Inc.).

Supporting Information

Supporting Information is available from the Wiley Online Library or from the author.

Acknowledgements

The authors thank Manuel Engelmayer and Prakhar Sahay (Universität Augsburg) for some technical support for these experiments. This research was partially supported by the Deutsche Forschungsgemeinschaft (DFG, Project nos. 341263954 & 432420985).

Open access funding enabled and organized by Projekt DEAL.

Conflict of Interest

The authors declare no conflict of interest.

Data Availability Statement

The data that support the findings of this study are available from the corresponding author upon reasonable request.

Keywords

charge accumulation, dipolar doping, exciton-polaron quenching, organic light-emitting diodes, spontaneous orientation polarization

Received: June 1, 2022
Revised: July 5, 2022
Published online: August 15, 2022

[1] B. Ruhstaller, S. A. Carter, S. Barth, H. Riel, W. Riess, J. C. Scott, *J. Appl. Phys.* **2001**, *89*, 4575.
[2] D. Y. Kondakov, J. R. Sandifer, C. W. Tang, R. H. Young, *J. Appl. Phys.* **2003**, *93*, 1108.
[3] C. Murawski, K. Leo, M. C. Gather, *Adv. Mater.* **2013**, *25*, 6801.
[4] S. Scholz, D. Kondakov, B. Lüssem, K. Leo, *Chem. Rev.* **2015**, *115*, 8449.
[5] Y. Noguchi, W. Brütting, H. Ishii, *Jpn. J. Appl. Phys.* **2019**, *58*, SF0801.
[6] J. S. Bangsund, J. R. Van Sambeek, N. M. Concannon, R. J. Holmes, *Sci. Adv.* **2020**, *6*, eabb2659.
[7] Y. Esaki, M. Tanaka, T. Matsushima, C. Adachi, *Adv. Electron. Mater.* **2021**, *7*, 2100486.
[8] E. O. Afolayan, I. Dursun, C. Lang, E. Pakhomenko, M. Kondakova, M. Boroson, M. Hickner, R. J. Holmes, N. C. Giebink, *Phys. Rev. Appl.* **2022**, *17*, L051002.
[9] Y. Noguchi, Y. Tanaka, H. Ishii, W. Brütting, *Synth. Met.* **2022**, *288*, 117101.
[10] S. Berleb, W. Brütting, G. Paasch, *Org. Electron.* **2000**, *1*, 41.
[11] W. Brütting, S. Berleb, A. G. Mückl, *Org. Electron.* **2001**, *2*, 1.
[12] A. Hofmann, M. Schmid, W. Brütting, *Adv. Opt. Mater.* **2021**, *9*, 2101004.
[13] K. Bagchi, N. E. Jackson, A. Gujral, C. Huang, M. F. Toney, L. Yu, J. J. De Pablo, M. D. Ediger, *J. Phys. Chem. Lett.* **2019**, *10*, 164.
[14] M. Tanaka, M. Auffray, H. Nakanotani, C. Adachi, *Nat. Mater.* **2022**, *21*, 819.
[15] Y. Noguchi, N. Sato, Y. Tanaka, Y. Nakayama, H. Ishii, *Appl. Phys. Lett.* **2008**, *92*, 203306.
[16] Y. Noguchi, Y. Miyazaki, Y. Tanaka, N. Sato, Y. Nakayama, T. D. Schmidt, W. Brütting, H. Ishii, *J. Appl. Phys.* **2012**, *111*, 114508.
[17] K. Osada, K. Goushi, H. Kaji, C. Adachi, H. Ishii, Y. Noguchi, *Org. Electron.* **2018**, *58*, 313.
[18] B. A. Naqvi, M. Schmid, E. Crovini, P. Sahay, T. Naujoks, F. Rodella, Z. Zhang, P. Strohriegl, S. Bräse, E. Zysman-Colman, W. Brütting, *Front. Chem.* **2020**, *8*, 750.
[19] S. Sato, M. Takada, D. Kawate, M. Takata, T. Kobayashi, H. Naito, *Jpn. J. Appl. Phys.* **2019**, *58*, SFFA02.
[20] Y. Noguchi, H. Lim, T. Isoshima, E. Ito, M. Hara, W. Won Chin, J. Wook Han, H. Kinjo, Y. Ozawa, Y. Nakayama, H. Ishii, *Appl. Phys. Lett.* **2013**, *102*, 203306.
[21] S. Altazin, S. Züfle, E. Knapp, C. Kirsch, T. D. Schmidt, L. Jäger, Y. Noguchi, W. Brütting, B. Ruhstaller, *Org. Electron.* **2016**, *39*, 244.
[22] A. J. L. Hofmann, S. Züfle, K. Shimizu, M. Schmid, V. Wessels, L. Jäger, S. Altazin, K. Ikegami, M. R. Khan, D. Neher, H. Ishii, B. Ruhstaller, W. Brütting, *Phys. Rev. Appl.* **2019**, *12*, 064052.
[23] Y. Tanaka, T. Makino, H. Ishii, *IEICE Trans. Electron.* **2019**, *E102-C*, 172.
[24] R. Coehoorn, X. Lin, C. H. L. Weijtens, S. Gottardi, H. van Eersel, *Phys. Rev. Appl.* **2021**, *16*, 034048.
[25] L. Jäger, T. D. Schmidt, W. Brütting, *AIP Adv.* **2016**, *6*, 095220.
[26] E. Ito, Y. Washizu, N. Hayashi, H. Ishii, N. Matsuie, K. Tsuboi, Y. Ouchi, Y. Harima, K. Yamashita, K. Seki, *J. Appl. Phys.* **2002**, *92*, 7306.
[27] W. Zou, R. Li, S. Zhang, Y. Liu, N. Wang, Y. Cao, Y. Miao, M. Xu, Q. Guo, D. Di, L. Zhang, C. Yi, F. Gao, R. H. Friend, J. Wang, W. Huang, *Nat. Commun.* **2018**, *9*, 608.
[28] S. Nowy, W. Ren, A. Elschner, W. Lövenich, W. Brütting, *J. Appl. Phys.* **2010**, *107*, 054501.
[29] T. Morgenstern, M. Schmid, A. Hofmann, M. Bierling, L. Jäger, W. Brütting, *ACS Appl. Mater. Interfaces* **2018**, *10*, 31541.
[30] Y. Noguchi, K. Osada, K. Ninomiya, H. D. C. N. Gunawardana, K. R. Koswattage, H. Ishii, *J. Soc. Inf. Disp.* **2021**, *29*, 29.
[31] P. Friederich, V. Rodin, F. Von Wrochem, W. Wenzel, *ACS Appl. Mater. Interfaces* **2018**, *10*, 1881.
[32] D. Taguchi, S. Inoue, L. Zhang, J. Li, M. Weis, T. Manaka, M. C. N. Iwamoto, *J. Phys. Chem. Lett.* **2010**, *1*, 803.
[33] Y. Ueda, H. Nakanotani, T. Hosokai, Y. Tanaka, H. Hamada, H. Ishii, S. Santo, C. Adachi, *Adv. Opt. Mater.* **2020**, *8*, 2000896.
[34] T. Matsushima, G.-H. Jin, Y. Kanai, T. Yokota, S. Kitada, T. Kishi, H. Murata, *Org. Electron.* **2011**, *12*, 520.
[35] A. P. Marchetti, K. E. Sassin, R. H. Young, L. J. Rothberg, D. Y. Kondakov, *J. Appl. Phys.* **2011**, *109*, 013709.
[36] S. Reineke, K. Walzer, K. Leo, *Phys. Rev. B* **2007**, *75*, 125328.
[37] K. W. Hershey, R. J. Holmes, **2017**, *195501*, 120.
[38] S. Oyama, H. Sakai, H. Murata, *Jpn. J. Appl. Phys.* **2016**, *55*, 03DD13.
[39] J. Kalinowski, W. Stampor, J. Mezyk, M. Cocchi, D. Virgili, V. Fattori, P. Di Marco, *Phys. Rev. B* **2002**, *66*, 235321.
[40] H. Yoshida, K. Yoshizaki, *Org. Electron.* **2015**, *20*, 24.
[41] T. D. Anthopoulos, J. P. J. Markham, E. B. Namdas, I. D. W. Samuel, S. C. Lo, P. L. Burn, *Appl. Phys. Lett.* **2003**, *82*, 4824.
[42] T. Tsutsui, C. Aminaka, C. P. Lin, D.-U. Kim, *Philos. Trans. R. Soc. A* **1997**, *355*, 801.
[43] H. H. Chou, C. H. Cheng, *Adv. Mater.* **2010**, *22*, 2468.
[44] G. Meng, X. Chen, X. Wang, N. Wang, T. Peng, S. Wang, *Adv. Opt. Mater.* **2019**, *7*, 1900130.

© 2022 The Authors. Advanced Optical Materials published by Wiley-VCH GmbH

21951071, 2022, 21, Downloaded from https://onlinelibrary.wiley.com/doi/10.1002/adom.202201278 by Universitaetsbibl Augsburg, Wiley Online Library on [06/11/2022]. See the Terms and Conditions (https://onlinelibrary.wiley.com/terms-and-conditions) on Wiley Online Library for rules of use; OA articles are governed by the applicable Creative Commons License

[45] M. Oehzelt, K. Akaike, N. Koch, G. Heimel, *Sci. Adv.* **2015**, *1*, e1501127.
[46] K. Akaike, *Jpn. J. Appl. Phys.* **2018**, 57, 03EA03.
[47] M. Kröger, S. Hamwi, J. Meyer, T. Dobbertin, T. Riedl, W. Kowalsky, H. H. Johannes, *Phys. Rev. B* **2007**, *75*, 235321.
[48] P. M. Borsenberger, E. H. Magin, M. Der Van Auweraer, F. C. De Schryver, *Phys. Status Solidi* **1993**, *140*, 9.
[49] M. Baldo, S. Forrest, *Phys. Rev. B* **2001**, *64*, 085201.
[50] J. C. Scott, *J. Vac. Sci. Technol. A Vacuum, Surfaces, Film.* **2003**, *21*, 521.

© 2022 The Authors. Advanced Optical Materials published by Wiley-VCH GmbH

21951071, 2022, 21, Downloaded from https://onlinelibrary.wiley.com/doi/10.1002/adom.202201278 by Universitaetsbibl Augsburg, Wiley Online Library on [06/11/2022]. See the Terms and Conditions (https://onlinelibrary.wiley.com/terms-and-conditions) on Wiley Online Library for rules of use; OA articles are governed by the applicable Creative Commons License